

# 1 Distinct Scaling Regimes of Energy Release Dynamics in the 2 Nighttime Magnetosphere

V. M. Uritsky<sup>1</sup>, E. Donovan<sup>1</sup>, A. J. Klimas<sup>2</sup>, and E. Spanswick<sup>1</sup>

3 Based on a spatiotemporal analysis of POLAR UVI  
4 images, we show that the auroral emission events that  
5 initiate equatorward of the isotropic boundary (IB) ob-  
6 tained from a time-dependent empirical model, have sys-  
7 tematically steeper power-law slopes of energy, power,  
8 area and lifetime probability distributions compared to  
9 the events that initiate poleward of the IB. The low-  
10 latitude group of events contains a distinct subpopulation  
11 of substorm-scale disturbances violating the power-law  
12 behavior, while the high latitude group is described by  
13 nearly perfect power-law statistics over the entire range  
14 of scales studied. The results obtained indicate that the  
15 inner and outer portions of the plasma sheet are charac-  
16 terized by substantially different scaling regimes of bursty  
17 energy dissipation suggestive of different physics in these  
18 regions.

## 1. Introduction

19 The activity of the nighttime auroral oval represents a  
20 wide range of dynamical processes in the magnetotail,  
21 including substorm expansion onsets, pseudobreakups,  
22 steady magnetospheric convection events with or with-  
23 out substorms, bursty bulk flows, and sawtooth events  
24 (see e.g., *Zesta et al.* [2000]; *Lui* [2001]; *Frey et al.* [2004];  
25 *Henderson et al.* [2006]). Despite the diversity of physical  
26 conditions associated with each particular type of auroral  
27 activity, their net energy output can be described by a  
28 set of apparently universal power-laws (*Lui et al.* [2000];  
29 *Lui* [2002]; *Uritsky et al.* [2003, 2002, 2006]) signaling  
30 the existence of a organizing dynamical principle arrang-  
31 ing intermittent magnetospheric dissipation across vast  
32 ranges of spatial and temporal scales.

33 Power-law intermittency of energy dissipation has at-  
34 tracted significant attention in modern statistical me-  
35 chanics (see *Dhar* [2006] and refs therein) and is often  
36 considered a hallmark of turbulent and/or critical phe-  
37 nomena with no characteristic scales other than those  
38 dictated by the finite size of the system (*Sreenivasan*  
39 *et al.* [2004]; *Lubeck* [2004]). Examples of such behav-  
40 ior in geo- and space sciences include fully developed  
41 turbulence in hydrodynamic or magnetized flows (*Lazar-*  
42 *ian* [2006]), Gutenberg-Richter statistics of earthquake  
43 magnitudes (*Turcotte* [1989]), scale-invariance in the so-  
44 lar corona (*Charbonneau et al.* [2001]). In this context,  
45 the auroral activity provides one of the most impressive

<sup>1</sup>Physics and Astronomy Department, University of  
Calgary, Calgary, AB, Canada

<sup>2</sup>UMBC at NASA / Goddard Space Flight Center,  
Greenbelt, Maryland, USA

46 examples of scale-free behavior in nature. The energy  
 47 distribution of electron emission regions exhibits a power-  
 48 law shape over a range of 6 orders of magnitude (*Uritsky*  
 49 *et al.* [2002]) which can be extended to up to 11 orders  
 50 by combining the satellite data with ground-based TV  
 51 observations (*Kozelov et al.* [2004]).

52 The auroral emission statistics reported so far repre-  
 53 sent global long-term properties of nighttime magneto-  
 54 spheric disturbances. The fact that these properties are  
 55 dominated by power-law scaling does not eliminate the  
 56 possibility of a more complex behavior on the level of  
 57 specific plasma sheet structures described by drastically  
 58 different physical conditions and geometry. In this study,  
 59 we are taking a step toward a better understanding of  
 60 the relationship between the scale-free auroral precipita-  
 61 tion statistics and the underlying central plasma sheet  
 62 (CPS) morphology. We suggest that the inner and the  
 63 outer CPS regions are responsible for three distinct scal-  
 64 ing modes of the auroral precipitation dynamics, and pro-  
 65 vide a possible physical interpretation for the observed  
 66 differences.

## 2. Data and Algorithm

67 We have studied time series of digital images of night-  
 68 time northern aurora (55-80 MLat, 2000 - 0400 MLT)  
 69 taken by the Ultraviolet Imager (UVI) onboard the PO-  
 70 LAR spacecraft in the 165.5 to 174.5 nm portion of the  
 71 Lyman-Birge-Hopfield spectral band (integration time  
 72 36.5 s, time resolution 184 s). The data analyzed in-  
 73 clude 16,000 images covering two observation periods:  
 74 01/01/1997 - 02/28/1997 and 01/01/1998 - 02/28/1998.  
 75 Our analysis was based on spatiotemporal tracking of auroral  
 76 emission events (*Uritsky et al.* [2002, 2003]). The  
 77 UV luminosity  $w(t, \mathbf{r})$  was studied as a function of time  $t$   
 78 and position  $\mathbf{r}$  on the image plane. First, active auroral  
 79 regions were identified by applying an activity threshold  
 80  $w_a$  representing a background UV flux. Contiguous spa-  
 81 tial regions with  $w(\mathbf{r}, t) > w_a$  were treated as pieces of  
 82 evolving events. Second, by checking for overlap of com-  
 83 mon pixels between each pair of consecutive UVI frames,  
 84 we constructed a set of spatiotemporal integration do-  
 85 mains  $\Lambda_i (i = 1, \dots, N)$  corresponding to each of  $N$  individ-  
 86 ual emission events found by our method. These domains  
 87 of contiguous activity in space and time were used to com-  
 88 pute the lifetime,  $T_i$ , the energy,  $E_i = k \int_{\Lambda_i} w(\mathbf{r}, t) d\mathbf{r} dt$ ,  
 89 the peak power,  $W_i = k \max_t (\int_{\Lambda_i(t)} w(\mathbf{r}, t) d\mathbf{r})$ , as well  
 90 the peak area,  $A_i = \max_t (\int_{\Lambda_i(t)} d\mathbf{r})$  of every event,  
 91 where  $k = 2.74 \times 10^{-8} \text{ J} \cdot \text{photon}^{-1}$  (*Brittnacher et al.*  
 92 [1997]) and the integrals were numerically approximated  
 93 by sums. The statistics reported below are for the thresh-  
 94 old  $w_a = 10 \text{ photons} \cdot \text{cm}^2 \cdot \text{s}^{-1}$ . Their main features re-  
 95 main the same if the threshold is varied at least within  
 96 the range 5 to 15  $\text{photons} \cdot \text{cm}^2 \cdot \text{s}^{-1}$ .

The auroral onset positions of each event were esti-  
 mated with an error of about 300 km in either spatial  
 direction. We organized the data to allow us to compare  
 events that likely originate in the inner magnetosphere  
 relative to events that likely originate in the outer mag-  
 netosphere. To accomplish this, we determine the event  
 locations relative to the isotropic boundary (IB) at the  
 meridian of the event origin <sup>1</sup>:

$$\phi_i = MLat_i - [A_0 - A_1 \cos(\pi(MLT_i - MLT_0)/12)] \quad (1)$$

97 Here,  $MLT_i$  and  $MLat_i$  are the onset coordinates of the

98  $i$ -th event.  $A_0$ ,  $A_1$ ,  $MLT_0$  are the coefficients of the empirical  
 99 IB model due to *Gvozdevsky and Sergeev* [1995]  
 100 which were computed based on hourly values of auroral  
 101 electrojet index (WDC for Geomagnetism, Kyoto) and  
 102 solar wind dynamic pressure (ACE spacecraft) at the be-  
 103 ginning of each auroral intensification. The ions main-  
 104 tain their isotropy on the poleward side of IB due to the  
 105 effective pitch angle scattering in the tail current sheet  
 106 (*Newell et al.* [1996]). As a result, the latitude of IB has  
 107 a high correlation with the magnetic field inclination at  
 108 the geomagnetic equator as well as with the equatorward  
 109 boundary of the proton aurora as determined from di-  
 110 rect optical observations (*Donovan et al.* [2003]). Here,  
 111 we have used the empirical IB model to separate inner  
 112 and outer emission events. Positive values of  $\phi$  on av-  
 113 erage indicate events originating on field lines that map  
 114 further out on the plasma sheet, as opposed to negative  
 115 values corresponding to the events that originate closer  
 116 to Earth.

117 The statistics of the emission events that initiated on  
 118 the poleward ( $\phi > 0$ ) and on the equatorward ( $\phi < 0$ )  
 119 side of the IB are characterized by sets of probability  
 120 density distributions  $p(x)$ , where  $x \in \{E, W, A, T\}$ . The  
 121 power-law exponents obtained from these distributions  
 122 are denoted as  $\tau_x$ , with the subscript indicating the vari-  
 123 able under study.

### 3. Results and Discussion

124 In the end we have 7481 events, 6231 and 1250 pole-  
 125 ward and equatorward of the IB, respectively. These  
 126 yielded a database of parameters  $E$ ,  $W$ ,  $A$ ,  $T$ ,  $MLT$ ,  
 127  $MLat$ ,  $\phi$  for those events. Figure 1 is the emission en-  
 128 ergy  $E$  as a function of the relative onset latitude  $\phi$   
 129 for all events ( $n = 7481$ ). The scatterplot has clear asym-  
 130 metric shape suggesting different statistics for negative  
 131 and positive  $\phi$  values. As we discuss below, these statis-  
 132 tical subsets are characterized by significantly different  
 133 regimes of scaling behavior indicating different physical  
 134 environments.

135 Figure 2 shows probability distributions for the events  
 136 which initiated on the poleward and equatorward sides  
 137 of the IB. The high-latitude (HL) events ( $\phi > 0$ ) ex-  
 138 hibit stable power-law distributions of emission energy  
 139  $E$ , peak emission power  $W$ , lifetime  $T$  and peak area  $A$   
 140 (not shown) with near-zero regression errors. The ranges  
 141 of scales of these power-law behaviors involves both small  
 142 auroral activations and large events whose energy output  
 143 lies in the range of global substorms. The exponents  $\tau_E$ ,  
 144  $\tau_W$ ,  $\tau_A$  and  $\tau_T$  are close to the values obtained earlier for  
 145 the same observation period without filtering the activity  
 146 by the onset location (*Uritsky et al.* [2002]).

147 The low-latitude (LL) events ( $\phi < 0$ ) have more com-  
 148 plicated statistical properties as can be expected from  
 149 Fig. 1. Their distribution functions demonstrate a  
 150 crossover behavior involving small-scale regions described  
 151 by  $\tau_x$  exponents which are greater than the correspond-  
 152 ing exponents of HL events, as well as large-scale regions  
 153 where the slopes are significantly shallower (the  $\tau_x$  expo-  
 154 nents for these regions are not well defined due to the in-  
 155 sufficient number of large-scale LL events). The position  
 156 of the crossover  $E^* = 5 \times 10^{12}$  J on the  $p(E)$  distribution  
 157 of LL events matches the data gap in Fig. 1 separating  
 158 low- and high-energy events with negative relative lati-  
 159 tudes  $\phi$ .

160 As can be seen from Table 1, only 1/6 of the events  
 161 contribute to the population with  $\phi < 0$ . However, their

162 participation in the energy budget of the electron aurora  
 163 approaches 50 percent as can be seen from the compar-  
 164 ison of the overall energy  $E_{tot}$  released by LL and HL  
 165 events. The fact that the HL events are the the most  
 166 common form of emission dynamics (relative occurrence  
 167 frequency 82.3%) is not a surprise as these events likely  
 168 map to the reconnection regions of the plasma sheet, as  
 169 we briefly discuss below. The table also shows that the  
 170 scaling behaviors of LL and LH events are described by  
 171 substantially different sets of  $\tau$  exponents.

172 Table 2 provides scaling exponents of energy distri-  
 173 butions  $p(E)$  as well as several parameters reflecting  
 174 the state of the solar wind and the auroral magneto-  
 175 sphere at the beginnings of emission events for four non-  
 176 overlapping ranges of magnetic latitude  $MLat$ . The data  
 177 show that the group of events that initiated southward of  
 178  $MLat=65$  are characterized by significantly higher statisti-  
 179 cal values of solar wind dynamic pressure and electrojet  
 180 index. These events seem to appear in a rather stretched  
 181 magnetotail configuration as reflected by the magneto-  
 182 tail (MT) index (*Gvozdevsky and Sergeev [1995]*). One  
 183 can also notice that the lower the magnetic latitude, the  
 184 higher is the exponent  $\tau_E$ . This tendency is in accordance  
 185 with the difference in the LL- and HL-event statistics re-  
 186 ported in Table 1, and it also suggests that the change  
 187 of the scaling regime of auroral emission events with on-  
 188 set latitude is a continuous process rather than a discrete  
 189 transition fully dictated by the empirical IB location.

190 From the statistical mechanics viewpoint, the exis-  
 191 tence of two or more scaling regimes within the same  
 192 physical system signals the presence of several distinct  
 193 universality classes (UC) in the underlying turbulent  
 194 dynamics (*Lubeck [2004]; Dhar [2006]*). It is known  
 195 that many stochastic scale-invariant phenomena can be  
 196 mapped onto a finite collection of such classes. This map-  
 197 ping is insensitive to a variety of physical parameters and  
 198 conditions and can be the same for quite different sys-  
 199 tems. Typically, each UC brings its own set of critical  
 200 exponents which express its inherent set of relevant vari-  
 201 ables and the underlying small- and large-scale symme-  
 202 tries (*BenHur and Biham [1996]*). In this context, our  
 203 results clearly show that the energy release dynamics in  
 204 the inner and outer CPS belong to different UCs and are  
 205 therefore governed by different physical mechanisms.

206 The nature of the isotropic boundary sheds some light  
 207 on the scaling regimes observed. On average, HL events  
 208 tend to initiate in the outer CPS region. The energy con-  
 209 version in this region is believed to be dominated by mag-  
 210 netic reconnection (*Birn and Hones [1981]*). Our results  
 211 strongly suggest that near-Earth (midtail) reconnection  
 212 is a turbulent bursty process with no well-defined dissipa-  
 213 tion scales. Judging by the relative occurrence of these  
 214 events (Table 1), the scale-free activity in the reconnec-  
 215 tion region is the dominant mode of energy release dy-  
 216 namics in the nightside magnetosphere. The power-law  
 217 emission exponents obtained for this region are rather  
 218 close to the exponents from a driven current sheet simula-  
 219 tion (*Klimas et al. [2004]*) consistent with multiscale tur-  
 220 bulent reconnection being the source of scale-invariance  
 221 in the outer CPS dynamics. The LL events are mainly  
 222 produced in the inner CPS. With a less stretched mag-  
 223 netic field topology, this region is not a region that favors  
 224 magnetic reconnection; however, it can be prone to cur-  
 225 rent disruption which offers an alternate mechanism for  
 226 energy release in the inner tail (*Lui [2000]*).

227 Our findings can be summarized as follows: (1) the  
 228 high-latitude emission events are characterized by broad-  
 229 band power-law statistics with no characteristic scales;

230 (2) the low-latitude events constitute a non-uniform sta-  
 231 tistical population with an energy crossover separating  
 232 large and small scale activity; (3) the scaling exponents  
 233 of the low- and high-latitude events are significantly dif-  
 234 ferent within the entire range of scales studied, which  
 235 signals distinct universality classes of energy release dy-  
 236 namics. To the extent that the empirical IB model can  
 237 be considered an accurate representation of the true IB,  
 238 the onsets of the HL events are located in an outer CPS  
 239 region, the onsets of the LL events in an inner CPS re-  
 240 gions, and these two regions exhibit distinctly different  
 241 energy release dynamics.

242 The difference in UC following from this analysis is  
 243 suggestive of different physics. It would be a significant  
 244 step forward if we could use physics-based models of CPS  
 245 dynamics to predict UCs, and to thereby determine how  
 246 the different statistical behaviors of the inner and outer  
 247 regions might be generated.

248 **Acknowledgments.** This work was partly supported by  
 249 NSERC operating grant of EFD. We thank William Liu for  
 250 stimulating discussions.

## Notes

1. A more accurate analysis based on Tsyganenko T96 and  
 T05 field-line models as well as optical determination of  
 the isotropic boundary will be published elsewhere.

## References

- 252 BenHur, A., and O. Biham (1996), Universality in sandpile  
 253 models, *Phys. Rev. E*, *53*(2), R1317–R1320.
- 254 Birn, J., and E. W. Hones (1981), 3-dimensional computer  
 255 modeling of dynamic reconnection in the geomagnetic tail,  
 256 *J. Geophys. Res.*, *86*(NA8), 6802–6808.
- 257 Brittnacher, M., R. Elsen, G. Parks, L. Chen, G. Germany,  
 258 and J. Spann (1997), A dayside auroral energy deposition  
 259 case study using the POLAR Ultraviolet imager, *Geophys-*  
 260 *ical Research Lett.*, *24*(8), 991–994.
- 261 Charbonneau, P., S. W. McIntosh, H. L. Liu, and T. J. Bog-  
 262 dan (2001), Avalanche models for solar flares, *Solar Phys.*,  
 263 *203*(2), 321–353.
- 264 Dhar, D. (2006), Theoretical studies of self-organized critical-  
 265 ity, *Physica A*, *369*(1), 29–70.
- 266 Donovan, E. F., B. J. Jackel, I. Voronkov, T. Sotirelis,  
 267 F. Creutzberg, and N. A. Nicholson (2003), Ground-based  
 268 optical determination of the b2i boundary: A basis for  
 269 an optical MT-index, *J. Geophys. Res.*, *108*(A3), doi:  
 270 10.1029/2001JA00919.
- 271 Frey, H. U., S. B. Mende, V. Angelopoulos, and E. F. Donovan  
 272 (2004), Substorm onset observations by IMAGE-FUV, *J.*  
 273 *Geophys. Res.*, *109*(A10), doi:10.1029/2004JA010607.
- 274 Gvozdevsky, B. B., and V. A. Sergeev (1995), MT-index  
 275 – A possible new index to characterize the configuration  
 276 of the magnetotail, *Three-Dimensional Magnetosphere*,  
 277 *18*(8), 51–54.
- 278 Henderson, M. G., et al. (2006), Substorms during the 10-11  
 279 August 2000 sawtooth event, *J. Geophys. Res.*, *111*(A6),  
 280 doi:10.1029/2005JA011366.
- 281 Klimas, A. J., V. M. Uritsky, D. Vassiliadis, and D. N.  
 282 Baker (2004), Reconnection and scale-free avalanching in  
 283 a driven current-sheet model, *J. Geophys. Res.*, *109*(A2),  
 284 doi:10.1029/2003JA010036.
- 285 Kozelov, B. V., V. M. Uritsky, and A. J. Klimas (2004), Power  
 286 law probability distributions of multiscale auroral dynamics  
 287 from ground-based TV observations, *Geophysical Research*  
 288 *Lett.*, *31*(20), doi:10.1029/2004GL020962.
- 289 Lazarian, A. (2006), Intermittency of magnetohydrodynamic  
 290 turbulence: An astrophysical perspective, *Int. J. Modern*  
 291 *Phys. D*, *15*(7), 1099–1111.

- 292 Lubeck, S. (2004), Universal scaling behavior of non-  
293 equilibrium phase transitions, *Int. J. Modern Phys. B*,  
294 *18*(31-32), 3977–4118.
- 295 Lui, A. T. Y. (2000), Electric current approach to magneto-  
296 spheric dynamics and the distinction between current dis-  
297 ruption and magnetic reconnection, in *AGU Monogr. Ser.*,  
298 vol. 118, edited by S. Ohtani, R. Fujii, M. Hesse, and R. L.  
299 Lysak, pp. 31–40, AGU, Washington, DC.
- 300 Lui, A. T. Y. (2001), Current controversies in magnetospheric  
301 physics, *Rev. Geophysics*, *39*(4), 535–563.
- 302 Lui, A. T. Y. (2002), Multiscale phenomena in the near-Earth  
303 magnetosphere, *J. Atmospheric Solar - Terrestrial Phys.*,  
304 *64*(2), 125–143.
- 305 Lui, A. T. Y., S. C. Chapman, K. Liou, and et al. (2000), Is the  
306 dynamic magnetosphere an avalanching system?, *Geophys.*  
307 *Res. Lett.*, *27*, 911–914.
- 308 Newell, P. T., Y. I. Feldstein, Y. I. Galperin, and C. I. Meng  
309 (1996), Morphology of nightside precipitation, *J. Geophys.*  
310 *Res.*, *101*(A5), 10,737–10,748.
- 311 Sreenivasan, K. R., A. Bershadskii, and J. J. Niemela (2004),  
312 Multiscale SOC in turbulent convection, *Physica A*, *340*(4),  
313 574–579.
- 314 Turcotte, D. L. (1989), Fractals in geology and geophysics,  
315 *Pure Appl. Geophysics*, *131*(1-2), 171–196.
- 316 Uritsky, V. M., A. J. Klimas, D. Vassiliadis, D. Chua, and  
317 G. Parks (2002), Scale-free statistics of spatiotemporal au-  
318 roral emissions as depicted by POLAR UVI images: Dy-  
319 namic magnetosphere is an avalanching system, *J. Geo-*  
320 *phys. Res.*, *107*(A12), doi:10.1029/2001JA000281.
- 321 Uritsky, V. M., A. J. Klimas, and D. Vassiliadis (2003), Eval-  
322 uation of spreading critical exponents from the spatiotem-  
323 poral evolution of emission regions in the nighttime aurora,  
324 *Geophys. Res. Lett.*, *30*(15), doi:10.1029/2002GL016556.
- 325 Uritsky, V. M., A. J. Klimas, and D. Vassiliadis (2006), Criti-  
326 cal finite-size scaling of energy and lifetime probability dis-  
327 tributions of auroral emissions, *Geophys. Res. Lett.*, *33*(8),  
328 doi:10.1029/2005GL025330.
- 329 Zesta, E., L. R. Lyons, and E. Donovan (2000), The auroral  
330 signature of Earthward flow bursts observed in the magne-  
331 totail, *Geophys. Res. Lett.*, *27*(20), 3241–3244.

---

332 V. M. Uritsky, Physics and Astronomy Department, Uni-  
333 versity of Calgary, SB605, 2500 University Drive NW, Calgary,  
334 AB T3A0P4, Canada. (vuritsky@phas.ucalgary.ca)

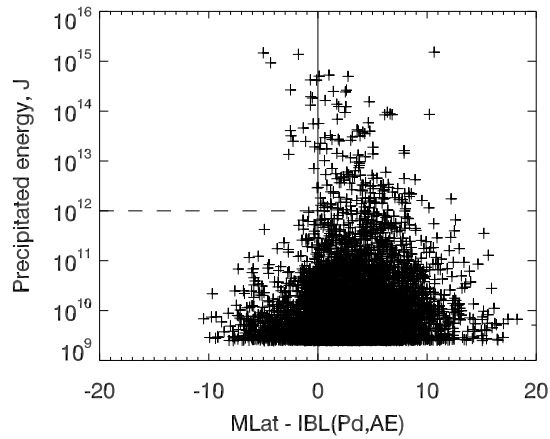


**Figure 1.** Scatterplot of emission energies  $E$  versus relative magnetic latitudes  $\phi$  of onset locations measured with respect to the empirical IB latitude (IBL) (see eq.(1)). The high-latitude ( $\phi > 0$ ) and the low-latitude ( $\phi < 0$ ) events contribute to two distinct scaling regimes of energy release dynamics in the nighttime magnetosphere as discussed further in the text. The dashed horizontal line marks the position of the crossover on the energy distribution shown in Fig. 2. The sharp lower cutoff is due to the fixed activity threshold  $w_a$ .

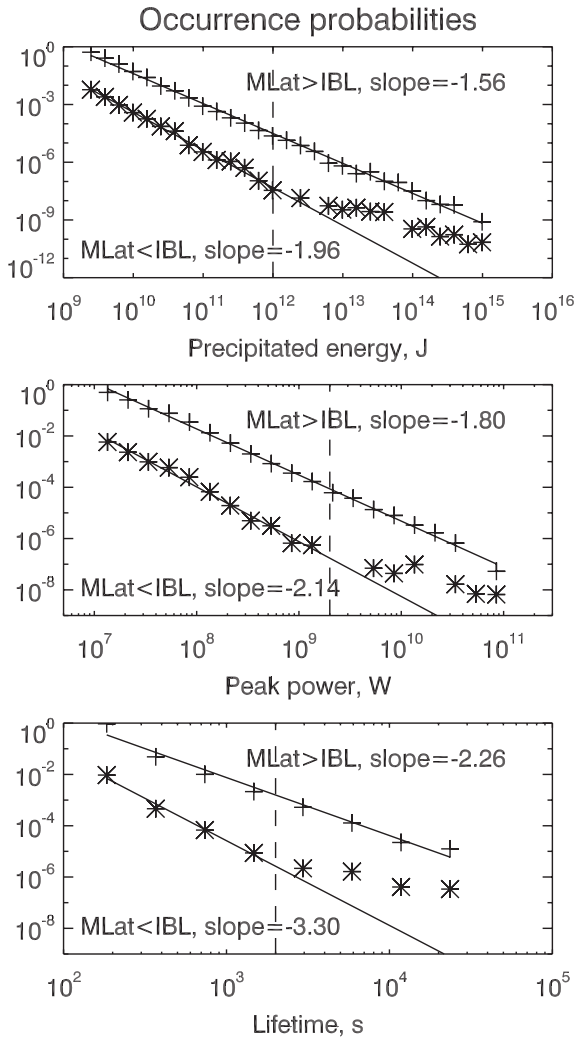


**Figure 2.** Probability distributions of energy  $E$ , peak power  $W$ , and lifetime  $T$  of auroral emission events initiated poleward ( $\phi > 0$ , crosses) and equatorward ( $\phi < 0$ , stars) of the empirical IB. The low-latitude distributions are shifted for easier comparison. The solid lines show the log-log distribution slopes for small-scale LL events (the power-law portions to the left of the dashed vertical lines) and for the entire group of HL events.

**Table 1.** Comparative characteristics of low- and high-latitude emission events.

Type of events	LL ( $\phi < 0$ )	HL ( $\phi > 0$ )
# of events	1250 (16.7%)	6231 (82.3%)
$E_{tot}, J$	$5.7 \times 10^{15}$ (47.5%)	$6.3 \times 10^{15}$ (52.5%)
$\tau_E$	$1.96 \pm 0.04$	$1.56 \pm 0.02$
$\tau_W$	$2.14 \pm 0.07$	$1.80 \pm 0.02$
$\tau_T$	$3.30 \pm 0.26$	$2.26 \pm 0.13$
$\tau_A$	$2.30 \pm 0.10$	$1.93 \pm 0.06$



**Table 2.** Scaling exponent  $\tau_E$  of emission events, solar wind dynamic pressure ( $P_d$ , auroral electrojet ( $AE$ ) index and the magnetotail ( $MT$ ) index (IB latitude at  $MLT=0$ , (eq. 1)), for four ranges of onset  $MLat$ .

$MLat$	$\tau_E$	$P_d$ , nPa	$AE$ , nT	$MT$
< 65	$2.06 \pm 0.04$	$2.64 \pm 0.05$	$206 \pm 5$	$63.2 \pm 0.03$
65...67	$1.88 \pm 0.04$	$2.42 \pm 0.03$	$106 \pm 3$	$63.9 \pm 0.03$
67...69	$1.59 \pm 0.03$	$2.41 \pm 0.03$	$84 \pm 3$	$64.0 \pm 0.03$
> 69	$1.58 \pm 0.03$	$2.20 \pm 0.03$	$93 \pm 4$	$64.1 \pm 0.03$